Journal of Molecular Catalysis A: Chemical 291 (2008) 38–48

Contents lists available at ScienceDirect

Journal of Molecular Catalysis A: Chemical

journal homepage: www.elsevier.com/locate/molcata

Theoretical study on selective oxidation of olefin and alcohol with Mo–peroxo amine complex using "paired interacting orbitals (PIOs)" analysis

Akinobu Shiga[a,c,*], Yasuhiko Kurusu[b]

[a] LUMMOX Lab, Japan
[b] Sophia University, Faculty of Science and Technology, 187-104, Honnmoku Mannsaka, Naka-ku, Yokohama 231-0833, Japan
[c] Takezono 2-18-4-302, Tsukuba, Ibaraki, 305-0032, Japan

ARTICLE INFO

Article history:
Received 13 December 2007
Received in revised form 18 May 2008
Accepted 19 May 2008
Available online 7 July 2008

Keywords:
Mo–peroxo complex
Olefin
Alcohol
Oxidation mechanism
Paired interacting orbitals (PIOs) analysis

ABSTRACT

Oxidation mechanisms of ethylene and methanol on $Mo(O)(OO)_2$ (an amine) and the influence of amines on the oxidation are studied by using paired interacting orbital (PIO) analysis of the transition states (TS) of the ethylene epoxidation and of the methanol coordinated complexes, the methoxy complexes, and the hydrogen abstraction of the methanol oxidation. In the case of ethylene oxidation, we are able to recognize three important PIOs: PIO-1 which expresses the electron delocalization from the π-orbital of the ethylene to the σ*-orbital(O^3–O^4) of the Mo peroxo; PIO-2 which expresses the electron delocalization from the p-orbital of O^4 of the Mo peroxo to the π*-orbital of the ethylene; and PIO-3 which expresses the overlap repulsion between the ethylene and occupied (Mo–O^3–O^4) orbitals of the Mo peroxo. This overlap repulsion is enhanced by the coordination of higher alkyl amines to the Mo peroxo, because of the destabilization of these occupied (Mo–O^3–O^4) orbitals. In the case of methanol oxidation, the main components of the PIO-1 of the methanol coordinated complexes and the methoxy complexes are Mo-4d orbitals of the unoccupied orbitals of the Mo peroxo part, and the main components of the PIO-1 of the hydrogen abstraction are O^5-2p, O^6-2p and C-2p orbitals of SOMO of the Mo peroxo part. The energy of the MOs, that contain these Mo-4d, O-2p or C-2p orbitals are not influenced by the amine coordination on the Mo atom. Results suggest that ethylene epoxidation is hindered by the coordination of higher alkyl amines on Mo peroxo complexes, whereas methanol oxidation is not hindered by the coordination of the amines.

1. Introduction

The epoxidation of olefins and the oxidation of alcohols to aldehydes and ketones by Mo peroxo complexes are important reactions in organic synthesis. Since the molybdenum is reoxidized by hydrogen peroxide and can be reused, the oxidation is environmentally benign. [1] One of the authors reported that cyclohexene oxide was predominantly obtained by oxidation of 1:1 mixtures of cyclohexene and 2-octanol with Mo–peroxo and primary amine systems, whereas methyl–hexylketone was mainly obtained with Mo–peroxo and tertiary amine systems [2]. We are interested in these reasons for the influence of the amines on this selective oxidation.

Many experimental and theoretical studies on olefin epoxidation mechanisms have been reported. [3] Two possible oxygen transfer processes that have been suggested are shown in Scheme 1.

Because of the recent DFT calculations, Route A, the concerted reaction course, is now becoming widely accepted. A concerted transfer of peroxo oxygen via spiro transition structures is postulated [3d]. No forming of olefin π-complex on Mo is observed in the route. How the olefin approaches the transition state is vague and the influence of amine ligands has not been described.

The oxidation mechanism of alcohol is also well established. The oxidation takes place via alcohol coordination to Mo, formation of Mo alkoxy complex and α-hydrogen abstraction from the alkoxy moiety. Deng and Ziegler reported a combination study of DFT calculation and an intrinsic reaction coordinate method of the methanol oxidation [4]. They used MO_2Cl_2 (M = Cr, Mo and W) as model oxo complexes, in which amines are not included. So the influence of amine ligands on alcohol oxidation is not discussed yet.

Here we study the following items:

(1) the influence of amines on ethylene epoxidation,
(2) the influences of amines on methanol coordination to Mo complex, on methoxy–Mo complex formation and on α-hydrogen abstraction from the methoxy moiety.

* Corresponding author.
E-mail addresses: aas55@mail2.accsnet.ne.jp (A. Shiga), GZS00125@nifty.ne.jp (Y. Kurusu).

1381-1169/$ – see front matter © 2008 Elsevier B.V. All rights reserved.
doi:10.1016/j.molcata.2008.05.012

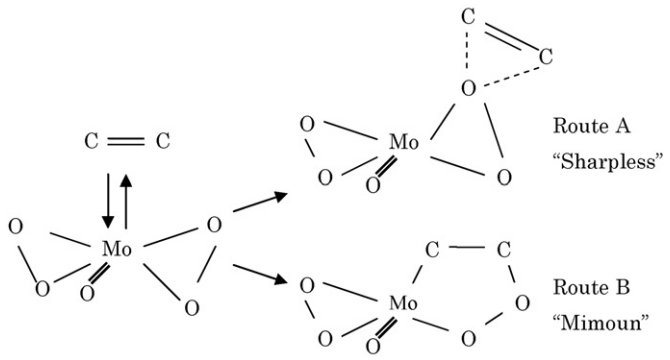

Scheme 1.

One goal of this study is to clarify the role of amines in olefin epoxidation and in alcohol oxidation and to discover the reason why a selective oxidation of alcohols is attained by addition of higher alkyl amines to the oxidation system.

2. Models and calculation methods

The starting molecules employed here are $Mo(O)(OO)_2$(amine: NH_3, NMe_3, NMe_2Et, $NMeEt_2$), ethylene, and methanol.

2.1. Generation of structures of TS of ethylene epoxidation on $Mo(O)(OO)_2$(amine), methanol coordination complex of $Mo(O)(OO)_2$(amine) and methoxy complex of $Mo(O)(OO)(OOH)$(amine)

We present the structures of $Mo(O)(OO)_2(OPH_3)$ and TS3 in supporting information [3j]. After replacing the OPH_3 with NH_3, we optimized the structures of the NH_3–Mo–diperoxo compound by RHF method (SBKJC ECP basis sets) using PC GAMESS developed by Dr. Alex A. Granovsky of the Laboratory of Chemical Cybernetics at Moscow State University [5]. We replaced the NH_3 molecule with another amines. We optimized the structure of the methanol coordination complex of $Mo(O)(OO)_2(NH_3)$ and the methoxy complex of $Mo(O)(OO)(OOH)(NH_3)$ by the above RHF method, and we replaced the NH_3 molecule with other amines.

2.2. PIO calculations

The paired interacting orbital (PIO) calculation proposed by Fujimoto et al. [6] is a method for unequivocally determining the orbitals which should play dominant roles in chemical interactions between two systems, [A] and [B], which construct a combined system [C]. In the case of the ethylene epoxidation, [C] is the ethylene complex, while [A] is the Mo–peroxo portion and [B] is the ethylene portion. The geometries of [A] and [B] are the same as those in the complex [C] ([A – B]≡[C]).

The extended Hückel MOs of [A], [B] and [C] are calculated. The extended Hückel parameters are given in the Appendix A. PIOs are obtained by applying the procedure that was proposed by Fujimoto et al. [6]. It is summarized as follows:

(1) we expand the MOs of a complex in terms of the MOs of two fragment species, to determine the expansion coefficients $c_{i,f}$, $c_{m+j,f}$ and $d_{k,f}$, $d_{n+l,f}$ in Eq. (1);

$$\Phi_f = \sum_{i=1}^{m} c_{i,f}\phi_i + \sum_{j=1}^{M-m} c_{m+j,f}\phi_{m+j} + \sum_{k=1}^{n} d_{k,f}\psi_k + \sum_{l=1}^{N-n} d_{n+l,f}\psi_{n+l}, \quad = 1, 2, \ldots, m+n, \tag{1}$$

(2) we construct an interaction matrix P which represents the interaction between the MOs of the fragment [A] and the MOs of the fragment [B];

$$P = \begin{pmatrix} p_{i,k} & p_{i,n+l} \\ p_{m+j,k} & p_{m+j,n+l} \end{pmatrix} \tag{2}$$

in which

$$p_{i,k} = n_{t,u}\sum_{f=1}^{m+n} c_{i,f}d_{k,f} \qquad i = 1 \sim m, \quad k = 1 \sim n$$

$$p_{i,n+l} = n_{t,u}\sum_{f=1}^{m+n} c_{i,f}d_{n+l,f} \qquad i = 1 \sim m, \quad l = 1 \sim N-n$$

$$p_{m+j,k} = n_{t,u}\sum_{f=1}^{m+n} c_{m+j,f}d_{k,f} \qquad j = 1 \sim M-m, \quad k = 1 \sim n$$

$$p_{m+j,n+l} = n_{t,u}\sum_{f=1}^{m+n} c_{m+j,f}d_{n+l,f} \qquad j = 1 \sim M-m, \quad l = 1 \sim N-n$$

(3) we obtain transformation matrix U^A (for A) and U^B (for B) by

$$\tilde{P}PU^A = U^A\Gamma \tag{3}$$

$$U^R_{s,\nu} = (\gamma_\nu)^{-1/2}\sum_{r}^{N} p_{r,s}U^A_{r,\nu} \quad \nu = 1, 2, \ldots, N \tag{4}$$

(4) and finally we obtain the PIOs by Eq. (5) and Eq. (6):

$$\phi'_\nu = \sum_{r}^{N} U^A_{r,\nu}\phi_r \quad \text{(for A)} \tag{5}$$

$$\psi'_\nu = \sum_{s}^{N} U^B_{s,\nu}\psi_s \quad \text{(for B)} \tag{6}$$

The $N \times M$ ($N < M$) orbital interactions in the complex C can thus be reduced to the interactions of N PIOs, N indicating the smaller of the numbers of MOs of the two fragments, A and B.

Although PIO analysis was proposed originally for ab initio calculations, we already reported that this approach was also useful in analyzing the results of extended Hückel MO calculations and was suitable for understanding reaction procedures in terms of orbital interactions, especially in catalytic systems that are large in size [8]. We also reported that relative catalytic activities deduced from PIO analysis based on extended Hückel MO calculations coincided with the order of activation energy obtained from ab initio MO calculations [9]. All calculations were carried out on the LUMMOX™ system [7].

3. Results

3.1. PIO analysis of TS of ethylene epoxidation: An influence of trans amines

As already described in Section 2.2, we divide each model [C] into two fragments, [A] and [B], here, [A] is the Mo peroxo portion and [B] is the ethylene portion. The fragmentation is shown in Fig. 1.

We executed PIO calculation of five TS models: **(1)** is TS3 in the reference [3j] and **(2)**–**(5)** are TS of amine versions: **(2)** is NH_3, **(3)** is NMe_3, **(4)** is NMe_2Et, and **(5)** is $NMeEt_2$, respectively,.

Eigen values of PIOs express a contribution of the PIOs to the interaction. The eigen values of PIOs of each model are summarized in Table 1. Table 1 tells us that the main interaction is expressed in

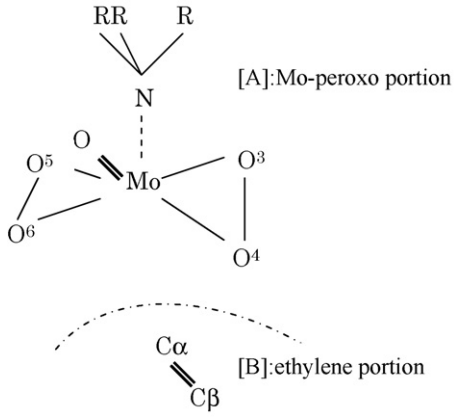

Fig. 1. The fragmentation of the models.

PIO-1, and that two other subsidiary interactions are expressed in PIO-2 and in PIO-3. The contributions of other PIOs are very small.

Contour maps of PIO-1, PIO-2 and PIO-3 of model **(1)**, **(2)**, **(4)** and **(5)**, projected on the *y*–*z* plane, and also contour maps of PIOs of out-of-phase overlap between the Mo peroxo part and the ethylene part of model **(1)**, **(2)**, **(4)** and **(5)**, projected on the *x*–*y* plane, are shown in Figs. 2 and 3, respectively.

We can visually understand that PIO-1 of models **(1)**, **(2)** and **(4)** express in-phase overlaps between π-orbital of the ethylene and σ*-orbital(O^3–O^4) of the Mo peroxo; however, PIO-1 of model **(5)** expresses a marked out-of-phase overlap between π-orbital of the ethylene and the occupied (Mo–O^4) orbitals of the Mo peroxo.

PIO-2 of models **(1)**, **(2)** and **(5)** express in-phase overlaps between π*-orbital of the ethylene and p-orbital of O^4 of the Mo peroxo; however, PIO-2 of model **(4)** expresses a marked out-of-phase overlap between the ethylene and occupied (Mo–O^3–O^4) orbitals of the Mo peroxo.

PIO-3 of models **(1)**, **(2)** and **(5)** express out-of-phase overlaps between the ethylene and occupied (Mo–O^3–O^4) orbitals of the Mo peroxo; however, PIO-3 of model **(4)** expresses in-phase overlap between π*-orbital of the ethylene and p-orbital of O^4 of the Mo peroxo.

Next, we precisely examine the PIO-1, PIO-2 and PIO-3 of model **(2)**.

The main components of the linear combination of the canonical MO (LCMO) representation of PIO-1 ((φ'_1, ψ'_1)), PIO-2 (φ'_2, ψ'_2) and PIO-3 (φ'_3, ψ'_3) of model **(2)** shown below, indicate that the Mo peroxo part of the PIO-1 is composed mainly of the LUMO and some subsidiary occupied orbitals, while the ethylene part of the PIO-1 is almost HOMO. On the contrary, the PIO-2 of the Mo part is composed of many occupied orbitals and the PIO-2 of the ethylene part contains not only LUMO but also some other occupied orbitals. The PIO-3 of the Mo part is mainly composed of occupied orbitals and the PIO-3 of the ethylene is also composed of occupied orbitals.

Model **(2)** of PIO-1: the Mo peroxo part,
$\varphi'_1 = -0.12\varphi_9 - 0.33\varphi_{11} + 0.12\varphi_{21}(\text{HOMO-1}) + 0.11\varphi_{22}(\text{HOMO}) + 0.89\varphi_{23}(\text{LUMO})$,
Model **(2)** of PIO-1: the ethylene part,
$\varphi'_1 = -0.12\Psi_5 - 0.99\psi_6(\text{HOMO})$.
Model **(2)** of PIO-2: the Mo peroxo part,
$\varphi'_2 = 0.12\varphi_4 - 0.15\varphi_{12} + 0.43\varphi_{13} + 0.13\varphi_{14} + 0.32\varphi_{17} - 0.66\varphi_{19} + 0.37\varphi_{20}(\text{HOMO-2})$
Model **(2)** of PIO-2: the ethylene part,
$\psi'_2 = -0.17\psi_1 + 0.37\psi_2 - 0.89\psi_7(\text{LUMO})$.
Model **(2)** of PIO-3: the Mo peroxo part,
$\varphi'_3 = -0.12\varphi_1 - 0.52\varphi_2 - 0.64\varphi_4 + 0.21\varphi_9 + 0.31\varphi_{11} + 0.13\varphi_{20}(\text{HOMO-2})$
$+ 0.15\varphi_{23}(\text{LUMO}) - 0.16\varphi_{32} + 0.14\varphi_{33}$
Model **(2)** of PIO-3: the ethylene part,
$\psi'_3 = 0.96\psi_1 - 0.10\psi_5 - 0.17\psi_7(\text{LUMO}) + 0.19\psi_{11}$.

The occupation numbers (ON) of the PIO-1, PIO-2 and PIO-3 are summarized in Table 2. The energy of φ_{23} (LUMO of the Mo peroxo of model **(2)**) is −12.86 eV, the energy of φ_{22} (HOMO of the Mo peroxo model **(2)**) is −13.82 eV and the energy of φ_{21} (HOMO-1 of Mo peroxo model **(2)**) is −13.98 eV. Since the energies of these MOs are very close and since all these MOs contain the same p-orbitals of O^4, they can easily mix in the PIO-1. So, the ON of the PIO-1 of the Mo part is larger than that of the ethylene; however, the total ON of the PIO-1 is very near to two. The PIO-1 expresses the electron delocalization from the ethylene to the Mo peroxo, the so called π-donation of ethylene. The ON of the PIO-2 of the Mo peroxo is large, near to two, and that of the ethylene is very small. The PIO-2 expresses the electron delocalization from the Mo peroxo to the ethylene and also includes some extents of repulsive occupied-occupied orbital interactions between the Mo peroxo and the ethylene. The ON of the PIO-3 of the Mo peroxo is large and that of the ethylene is also large. The PIO-3 mainly expresses the overlap repulsion between the Mo peroxo and the ethylene.

Based on the LCMO representation of PIOs, we can obtain the linear combination of atomic orbitals (LCAO) representation of the PIOs. LCAO representations of the PIO-1, PIO-2 and PIO-3 of model **(1)** and model **(2)** are shown below. They are almost coincident with each other.

Model **(1)** of PIO-1: the Mo peroxo part,
$\varphi'_1 = -0.16\text{Mo4}d_x - 0.10\text{Mo4}d_{xy} + 0.44\text{O}^3 2p_y + 0.33\text{O}^4 2p_x + 0.85\text{O}^4 2p_y - 0.17\text{O}^4 2p_z$,
Model **(1)** of PIO-1: the ethylene part,
$\psi'_1 = -0.18\text{C}^\alpha 2p_x - 0.59\text{C}^\alpha 2p_y + 0.11\text{C}^\alpha 2p_z - 0.19\,\text{C}^\beta 2p_x - 0.59\text{C}^\beta 2p_y + 0.09\text{C}^\beta 2p_z$,
Model **(1)** of PIO-2: the Mo peroxo part,
$\varphi'_2 = 0.11\text{Mo4}d_{yz} + 0.10\text{O}^3 2p_z + 0.10\text{O}^4 2s - 0.44\text{O}^4 2p_x - 0.84\text{O}^4 2p_z$,
Model **(1)** of PIO-2: the ethylene part,
$\psi'_2 = -0.12\text{C}^\alpha 2s - 0.14\text{C}^\alpha 2p_x - 0.71\text{C}^\alpha 2p_y + 0.25\text{C}^\alpha 2p_z + 0.28\text{C}^\beta 2p_x + 0.68\text{C}^\beta 2p_y$
$+ 0.14\text{H}^1 1s + 0.11\text{H}^2 1s - 0.20\text{H}^3 1s - 0.19\text{H}^4 1s$,
Model **(1)** of PIO-3: the Mo peroxo part,
$\varphi'_3 = -0.22\text{Mo5}s + 0.35\text{Mo5}p_y + 0.17\text{Mo4}d_{x2-y2} + 0.10\text{Mo4}d_{z2} + 0.10\text{Mo4}d_{xy}$
$+ 0.10\text{O}^3 2s - 0.32\text{O}^3 2p_y - 0.64\text{O}^4 2s + 0.21\text{O}^4 2p_y - 0.18\text{O}^4 2p_z$,
Model **(1)** of PIO-3: the ethylene part,
$\psi'_3 = 0.30\text{C}^\alpha 2s - 0.14\text{C}^\alpha 2p_x - 0.10\text{C}^\alpha 2p_y - 0.13\text{C}^\alpha 2p_z + 0.35\text{C}^\beta 2s + 0.18\text{C}^\beta 2p_y$
$+ 0.18\text{C}^\beta 2p_z + 0.22\text{H}^1 1s + 0.21\text{H}^2 1s + 0.15\text{H}^3 1s + 0.19\text{H}^4 1s$.

Model **(2)** of PIO-1: the Mo peroxo part,
$\varphi'_1 = 0.14\text{Mo4}d_{x2-y2} + 0.11\text{Mo4}d_{xy} - 0.44\text{O}^3 2p_y - 0.33\text{O}^4 2p_x - 0.85\text{O}^4 2p_y$
$+ 0.17\text{O}^4 2p_z$,
Model **(2)** of PIO-1: the ethylene part,
$\psi'_1 = 0.18\text{C}^\alpha 2p_x + 0.59\text{C}^\alpha 2p_y - 0.11\text{C}^\alpha 2p_z + 0.19\text{C}^\beta 2p_x + 0.59\text{C}^\beta 2p_y - 0.09\text{C}^\beta 2p_z$,
Model **(2)** of PIO-2: the Mo peroxo part,
$\varphi'_2 = 0.11\text{Mo4}d_{yz} + 0.10\text{O}^3 2p_z + 0.11\text{O}^4 2s - 0.44\text{O}^4 2p_x - 0.84\text{O}^4 2p_z$,
Model **(2)** of PIO-2: the ethylene part,
$\psi'_2 = -0.12\text{C}^\alpha 2s - 0.14\text{C}^\alpha 2p_x - 0.71\text{C}^\alpha 2p_y + 0.25\text{C}^\alpha 2p_z + 0.28\text{C}^\beta 2p_x + 0.68\text{C}^\beta 2p_y +$
$0.14\text{H}^1 1s + 0.11\text{H}^2 1s - 0.20\text{H}^3 1s - 0.19\text{H}^4 1s$,

Table 1
The eigen values of PIOs of each TS model of ethylene epoxidation

	Model				
	(1)	**(2)**	**(3)**	**(4)**	**(5)**
PIO-1	0.713	0.714	0.715	0.750	0.296
PIO-2	0.038	0.038	0.038	0.040	0.038
PIO-3	0.037	0.037	0.037	0.038	0.009
PIO-4	0.008	0.008	0.008	0.008	0.007
PIO-5	0.003	0.003	0.003	0.003	0.003
PIO-6	0.000	0.000	0.000	0.000	0.001
...	...	...	...	...	...
PIO-11	0.000	0.000	0.000	0.000	0.0000
PIO-12	0.000	0.000	0.000	0.000	0.0000

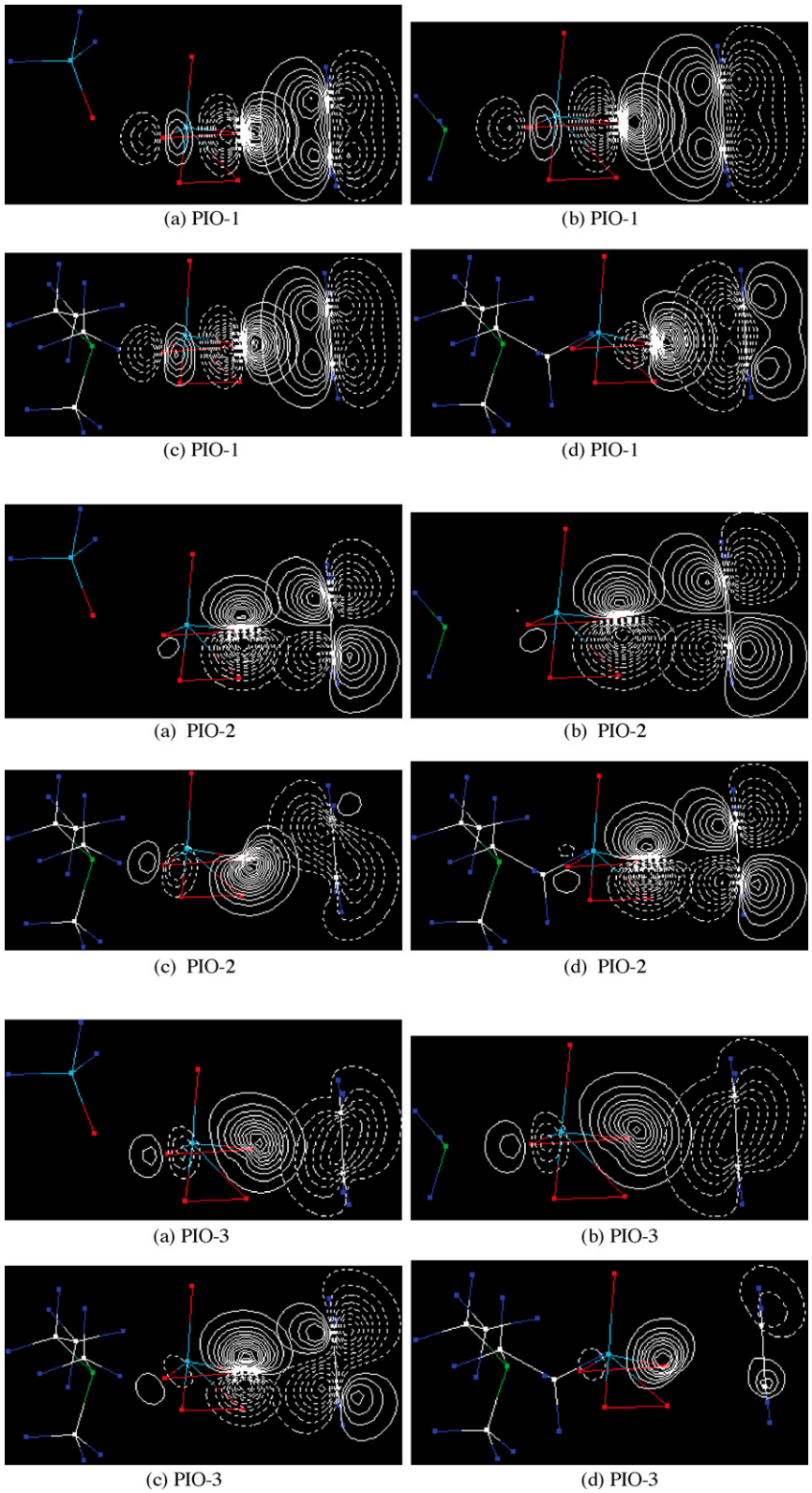

Fig. 2. Contour maps of PIO-1, PIO-2 and PIO-3 of (a) model **(1)**, (b) model **(2)**, (c) model **(4)** and (d) model **(5)**, projected on the *y*–*z* plane.

Model **(2)** of PIO-3: the Mo peroxo part,
$\varphi'_3 = -0.22\mathrm{Mo5s} + 0.36\mathrm{Mo5p}_y + 0.16\mathrm{Mo4d}_{x2-y2} + 0.10\mathrm{Mo4d}_{z2} + 0.11\mathrm{Mo4d}_{xy} + 0.10\mathrm{O}^3 2\mathrm{s} - 0.32\mathrm{O}^3 2\mathrm{p}_y - 0.64\mathrm{O}^4 2\mathrm{s} + 0.21\mathrm{O}^4 2\mathrm{p}_y - 0.18\mathrm{O}^4 2\mathrm{p}_z$,
Model **(2)** of PIO-3: the ethylene part,
$\psi'_3 = 0.30\mathrm{C}^\alpha 2\mathrm{s} - 0.14\mathrm{C}^\alpha 2\mathrm{p}_x - 0.10\mathrm{C}^\alpha 2\mathrm{p}_y - 0.13\mathrm{C}^\alpha 2\mathrm{p}_z + 0.35\mathrm{C}^\beta 2\mathrm{s} + 0.18\mathrm{C}^\beta 2\mathrm{p}_y + 0.18\mathrm{C}^\beta 2\mathrm{p}_z + 0.22\mathrm{H}^1 1\mathrm{s} + 0.21\mathrm{H}^2 1\mathrm{s} + 0.15\mathrm{H}^3 1\mathrm{s} + 0.19\mathrm{H}^4 1\mathrm{s}$.

Next, we examine the influence of the trans ligand on the interaction between the Mo peroxo part and the ethylene part.

The overlap populations of the PIO-1, PIO-2 and PIO-3 of each model are summarized in Table 3. The larger the overlap population is, the larger the reactivity of the reaction is. The overlap popula-

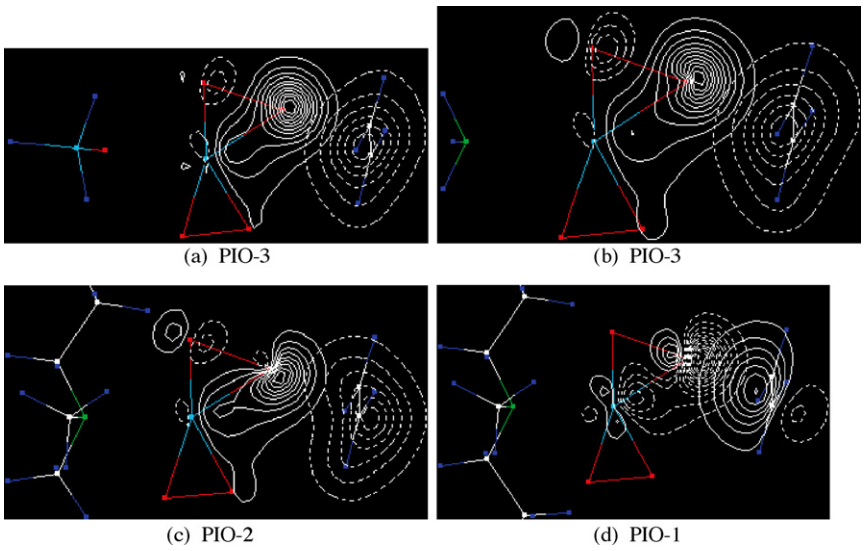

Fig. 3. Contour maps of PIOs of the out-of-phase overlap between the Mo peroxo part and the ethylene part of (a) model **(1)**, (b) model **(2)**, (c) model **(4)**, and (d) model **(5)**, projected on the *x*–*y* plane.

Table 2
The occupation numbers (ON) of the PIO-1, PIO-2 and PIO-3 of each TS model of ethylene epoxidation

	PIO-1			PIO-2			PIO-3		
	Mo peroxo	C_2H_4	Total	Mo peroxo	C_2H_4	Total	Mo peroxo	C_2H_4	Total
(1)	1.35	0.68	2.03	1.96	0.38	2.34	1.83	1.86	3.69
(2)	1.35	0.69	2.04	1.96	0.38	2.34	1.83	1.86	3.69
(3)	1.35	0.69	2.04	1.96	0.39	2.35	1.83	1.85	3.68
(4)	1.30	0.73	2.03	1.85	1.60	3.45	1.94	0.63	2.57
(5)	1.64	1.96	3.60	1.96	0.32	2.28	1.76	1.97	3.73

tions (OP) of the PIO-1, PIO-2 and PIO-3 of model **(1)**, model **(2)** and model **(3)** are almost the same. On the other hand, the overlap populations (ΣOP) of model **(4)** and model **(5)** markedly decrease. This difference suggests that the ethylene epoxidation takes place favorably on models **(1)**, **(2)** and **(3)**, while the epoxidation is hindered on model **(4)** and **(5)**.

In the cases of models **(1)**, **(2)** and **(3)**, the overlap repulsion is expressed in PIO-3, whereas in the case of model **(4)** the overlap repulsion is expressed in PIO-2, and further in the case of model **(5)** the repulsive interaction is expressed in PIO-1. The contribution of the overlap repulsion markedly increases in models **(4)** and **(5)**. Why does the overlap repulsion markedly increase in these models? The LCAO representations of PIO-3 of model **(2)**, PIO-2 of model **(4)** and PIO-1 of model **(5)** are shown below:

LCAO representation of model **(2)** of PIO-3: the Mo peroxo part,
$\varphi'_3 = -0.22\mathrm{Mo5s} + 0.36\mathrm{Mo5p}_y + 0.16\mathrm{Mo4d}_{x2-y2} + 0.10\mathrm{Mo4d}_{z2} + 0.11\mathrm{Mo4d}_{xy} + 0.10\mathrm{O}^3\mathrm{2s} - 0.32\mathrm{O}^3\mathrm{2p}_y - 0.64\mathrm{O}^4\mathrm{2s} + 0.21\mathrm{O}^4\mathrm{2p}_y - 0.18\mathrm{O}^4\mathrm{2p}_z,$
LCAO representation of model **(2)** of PIO-3: the ethylene part,
$\psi'_3 = 0.30\mathrm{C}^\alpha\mathrm{2s} - 0.14\mathrm{C}^\alpha\mathrm{2p}_x - 0.10\mathrm{C}^\alpha\mathrm{2p}_y - 0.13\mathrm{C}^\alpha\mathrm{2p}_z + 0.35\mathrm{C}^\beta\mathrm{2s} + 0.18\mathrm{C}^\beta\mathrm{2p}_y + 0.18\mathrm{C}^\beta\mathrm{2p}_z + 0.22\mathrm{H}^1\mathrm{1s} + 0.21\mathrm{H}^2\mathrm{1s} + 0.15\mathrm{H}^3\mathrm{1s} + 0.19\mathrm{H}^4\mathrm{1s},$

Table 3
The overlap populations (OP) of the PIO-1, PIO-2 and PIO-3 of each TS model of ethylene epoxidation

	PIO-1	PIO-2	PIO-3	ΣOP of PIO-1, -2 and -3
(1)	0.1874	0.0202	−0.0441	0.1635
(2)	0.1874	0.0202	−0.0440	0.1636
(3)	0.1873	0.0200	−0.0439	0.1636
(4)	0.1804	−0.0342	0.0089	0.1551
(5)	−0.2487	0.0225	−0.0090	−0.2353

LCAO representation of model **(4)** of PIO-2: the Mo peroxo part,
$\varphi'_2 = -0.20\mathrm{Mo5s} + 0.31\mathrm{Mo5p}_y + 0.13\mathrm{Mo4d}_{x2-y2} - 0.13\mathrm{O}^3\mathrm{2p}_x - 0.31\mathrm{O}^3\mathrm{2p}_y - 0.57\mathrm{O}^4\mathrm{2s} + 0.21\mathrm{O}^4\mathrm{2p}_x + 0.25\mathrm{O}^4\mathrm{2p}_y + 0.35\mathrm{O}^4\mathrm{2p}_z,$
LCAO representation of model **(4)** of PIO-2: the ethylene part,
$\psi'_2 = 0.31\mathrm{C}^\alpha\mathrm{2s} + 0.34\mathrm{C}^a\mathrm{2p}_y - 0.26\mathrm{C}^a\mathrm{2p}_z + 0.27\mathrm{C}^\beta\mathrm{2s} - 0.28\mathrm{C}^b\mathrm{2p}_y + 0.17\mathrm{C}^\beta\mathrm{2p}_z + 0.11\mathrm{H}^1\mathrm{1s} + 0.11\mathrm{H}^2\mathrm{1s} + 0.25\mathrm{H}^3\mathrm{1s} + 0.26\mathrm{H}^4\mathrm{1s},$
LCAO representation of model **(5)** of PIO-1: the Mo peroxo part,
$\varphi'_2 = -0.19\mathrm{Mo5s} - 0.13\mathrm{Mo5p}_x + 0.31\mathrm{Mo5p}_y + 0.22\mathrm{Mo4d}_{x2-y2} + 0.12\mathrm{Mo4}d_{z2} + 0.19\mathrm{Mo4d}_{xy} - 0.39\mathrm{O}^4\mathrm{2s} + 0.12\mathrm{O}^4\mathrm{2p}_x + 0.71\mathrm{O}^4\mathrm{2}p_y,$
LCAO representation of model **(5)** of PIO-1: the ethylene part,
$\psi'_2 = 0.15\mathrm{C}^\alpha\mathrm{2s} + 0.51\mathrm{C}^a\mathrm{2p}_y - 0.25\mathrm{C}^\alpha\mathrm{2p}_z + 0.15\mathrm{C}^\beta\mathrm{2s} + 0.23\mathrm{C}^\beta\mathrm{2p}_x + 0.50\mathrm{C}^b\mathrm{2p}_y + 0.11\mathrm{H}^1\mathrm{1s} + 0.08\mathrm{H}^2\mathrm{1s} + 0.11\mathrm{H}^3\mathrm{1s} + 0.09\mathrm{H}^4\mathrm{1s}.$

Comparing the PIO-2 of model **(4)** or the PIO-1 of model **(5)** with the PIO-3 of model **(2)**, we can observe increasing of contributions of ***O⁴2p*** orbitals(bold italic) and ethylene ***C 2p*** orbitals(bold italic). The destabilization of MOs containing Mo and $O^4$2p orbitals, caused by the coordination of NMe_2Et or $NMeEt_2$ to the Mo atom, enhances the overlap repulsion between O^4 2p orbitals and ethylene C 2p orbitals. The destabilization is larger in $NMeEt_2$ than in NMe_2Et.

3.2. An influence of trans amines on methanol oxidation

It is widely accepted that alcohol oxidation on Mo–peroxo complex proceeds via alcohol coordination, formation of alkoxy complex and hydrogen extraction of the alkoxy complex. We obtained methanol-coordinated complexes and methoxy com-

Table 4
The eigen values of PIOs of each Mo peroxo methanol complex and each methoxy complex

	Model							
	(6)	**(7)**	**(8)**	**(9)**	**(10)**	**(11)**	**(12)**	**(13)**
PIO-1	0.014	0.013	0.013	0.013	0.203	0.202	0.204	0.202
PIO-2	0.003	0.003	0.003	0.003	0.045	0.045	0.045	0.045
PIO-3	0.001	0.001	0.001	0.001	0.023	0.023	0.024	0.023
PIO-4	0.000	0.000	0.000	0.000	0.011	0.011	0.011	0.011
PIO-5	0.000	0.000	0.000	0.000	0.003	0.003	0.003	0.003
PIO-6	0.000	0.000	0.000	0.000	0.001	0.001	0.001	0.001
...	...	...	...	...	...			

plexes of the $(Mo(O)(OO)_2(amine)$. We executed PIO calculations of Mo peroxo methanol-coordinated complexes, **(6)**–**(9)**: model **(6)** is NH_3, **(7)** is NMe_3, **(8)** is NMe_2Et, and **(9)** is $NMeEt_2$, and Mo peroxo methoxy complexes, **(10)**–**(13)**: model **(10)** is NH_3, **(11)** is NMe_3, **(12)** is NMe_2Et, and **(13)** is $NMeEt_2$, respectively.

3.2.1. Methanol coordination

We executed PIO calculations of Mo peroxo methanol coordinated complexes, model **(6)**–**(9)**.

The eigen values of PIOs of each model are summarized in Table 4. Table 4 tells us that main interaction is expressed in PIO-1, and two other subsidiary interactions are expressed in PIO-2 and in PIO-3. The contribution of other PIOs is very small.

Contour maps of PIO-1, PIO-2 and PIO-3 of methanol coordinated complexes: models **(6)**, **(7)**, **(8)** and **(9)**, are shown in Fig. 4. They are very similar to each other.

The occupation numbers (ON) of the PIO-1, PIO-2 and PIO-3 of models **(6)**, **(7)**, **(8)** and **(9)** are summarized in Table 5. They are very close to each other.

The overlap populations of the PIO-1, PIO-2 and PIO-3 of models **(6)**, **(7)**, **(8)** and **(9)** are summarized in Table 6. They are also very close to each other.

The main components of the linear combination of canonical MO (LCMO) representation of PIO-1 (φ'_1, ψ'_1), PIO-2 (φ'_2, ψ'_2) and PIO-3 (φ'_3, ψ'_3) of model **(6)** are shown below. The PIO-1 of model **(6)** indicates that the Mo peroxo part of the PIO-1 is composed of unoccupied orbitals, while the methanol part of the PIO-1 is composed of occupied orbitals. The PIO-1 of model **(6)** expresses electron delocalization from the methanol to the Mo peroxo part. On the contrary, the PIO-2 of the model **(6)** indicates that the Mo part is composed of many occupied orbitals and several unoccupied orbitals and that the methanol part is composed of occupied orbitals. The PIO-2 of model **(6)** expresses mixtures of the overlap repulsion between the methanol and the Mo peroxo part and the electron delocalization from the methanol to the Mo peroxo complex. The PIO-3 of model **(6)** indicates that the Mo part is composed of occupied orbitals and the methanol part is composed of occupied orbitals and LUMO. The PIO-3 of model **(6)** expresses mixtures of the overlap repulsion between the methanol and the Mo peroxo part and the electron delocalization from the Mo peroxo part to the methanol.

Model **(6)** PIO-1: the Mo peroxo part,
$\varphi'_1 =$
$-0.60\varphi_{23}(\text{LUMO}) + 0.43\varphi_{25} + 0.36\varphi_{27}$,
Model **(6)** PIO-1: the methanol part,
$\psi'_1 =$
$-0.47\psi_5 + 0.75\psi_6 - 0.22\psi_7(\text{HOMO})$.
Model **(6)** PIO-2: the Mo peroxo part,
$\varphi'_2 =$
$0.47\varphi_4 - 0.44\varphi_7 + 0.20\varphi_{13} + 0.19\varphi_{15} - 0.19\varphi_{18} - 0.20\varphi_{21}(\text{HOMO-1}) + 0.29\varphi_{23}(\text{LUMO}) - 0.22\varphi_{25} - 0.21\varphi_{27}$,
Model **(6)** PIO-2: the methanol part,
$\psi'_2 =$
$0.71\psi_1 + 0.28\psi_4 - 0.29\psi_5 - 0.50\psi_6(\text{HOMO-1})$.
Model **(6)** PIO-3: the Mo peroxo part,
$\varphi'_3 =$
$0.38\varphi_2 + 0.50\varphi_5 + 0.33\varphi_8 + 0.40\varphi_{10} - 0.35\varphi_{12} + 0.30\varphi_{22}(\text{HOMO})$
Model **(6)** PIO-3: the methanol part,
$\psi'_3 =$
$-0.54\psi_2 - 0.73\psi_3 + 0.25\psi_8(\text{LUMO})$.

Based on the LCMO representation of PIOs, we can obtain the linear combination of atomic orbitals (LCAO) representation of the PIOs. We compared the LCAO representations of the PIO-1 of model **(6)** with the LCAO representations of the PIO-1 of model **(9)**. They are almost coincident with each other.

Model **(6)** of PIO-1: the Mo peroxo part,
$\varphi'_1 = -0.48O^1 2p_y + 0.32Mo5p_y -$
$0.35Mo4d_{x2-y2} - 0.24Mo4d_{z2} +$
$0.48Mo4d_{yz} - 0.25O^4 2s - 0.30O^4 2p_z -$
$0.27O^6 2s - 0.31O^6 2p_z - 0.20N2p_y$,
Model **(6)** of PIO-1: the methanol part,
$\psi'_1 = 0.30O2s - 0.92O2p_y - 0.20O2p_z$,
Model **(9)** of PIO-1: the Mo peroxo part,
$\varphi'_1 = -0.47O^1 2p_y - 0.33Mo5p_y +$
$0.30Mo4d_{x2-y2} + 0.23Mo4d_{z2} -$
$0.46Mo4d_{yz} + 0.26O42s +$
$0.30O^4 2p_z + 0.28O^6 2s + 0.31O^6 2p_z -$
$0.29N2p_y$,
Model **(9)** of PIO-1: the methanol part,
$\psi'_1 =$
$-0.31O2s + 0.92O2p_y + 0.20O2p_z$,

Such results suggest that the influence of amines on the methanol coordination is small.

3.2.2. Methoxy complex formation

We executed PIO calculations of Mo peroxo methoxy complexes: model **(10)**–**(13)**.

The eigen values of PIOs of the above each model are also summarized in Table 4. Table 4 tells us that the main interaction is expressed in PIO-1, and that two other subsidiary interactions are expressed in PIO-2 and in PIO-3. The contributions of other PIOs are very small.

Table 5
The occupation numbers (ON) of the PIO-1, PIO-2 and PIO-3 of each Mo peroxo methanol complex and each methoxy complex

	PIO-1			PIO-2			PIO-3		
	Mo peroxo	C_2H_4	Total	Mo peroxo	C_2H_4	Total	Mo peroxo	C_2H_4	Total
(6)	0.52	1.97	2.49	1.50	1.87	3.37	1.85	1.86	3.71
(7)	0.57	1.97	2.54	1.46	1.87	3.33	1.85	1.86	3.71
(8)	0.58	1.97	2.55	1.45	1.87	3.32	1.85	1.86	3.71
(9)	0.58	1.97	2.55	1.45	1.87	3.32	1.85	1.86	3.71
(10)	0.43	1.78	2.21	0.64	1.94	2.58	1.17	1.86	3.03
(11)	0.44	1.78	2.22	0.66	1.93	2.59	1.15	1.86	3.01
(12)	0.43	1.78	2.21	0.61	1.94	2.55	1.19	1.86	3.05
(13)	0.44	1.78	2.22	0.66	1.93	2.59	1.15	1.86	3.01

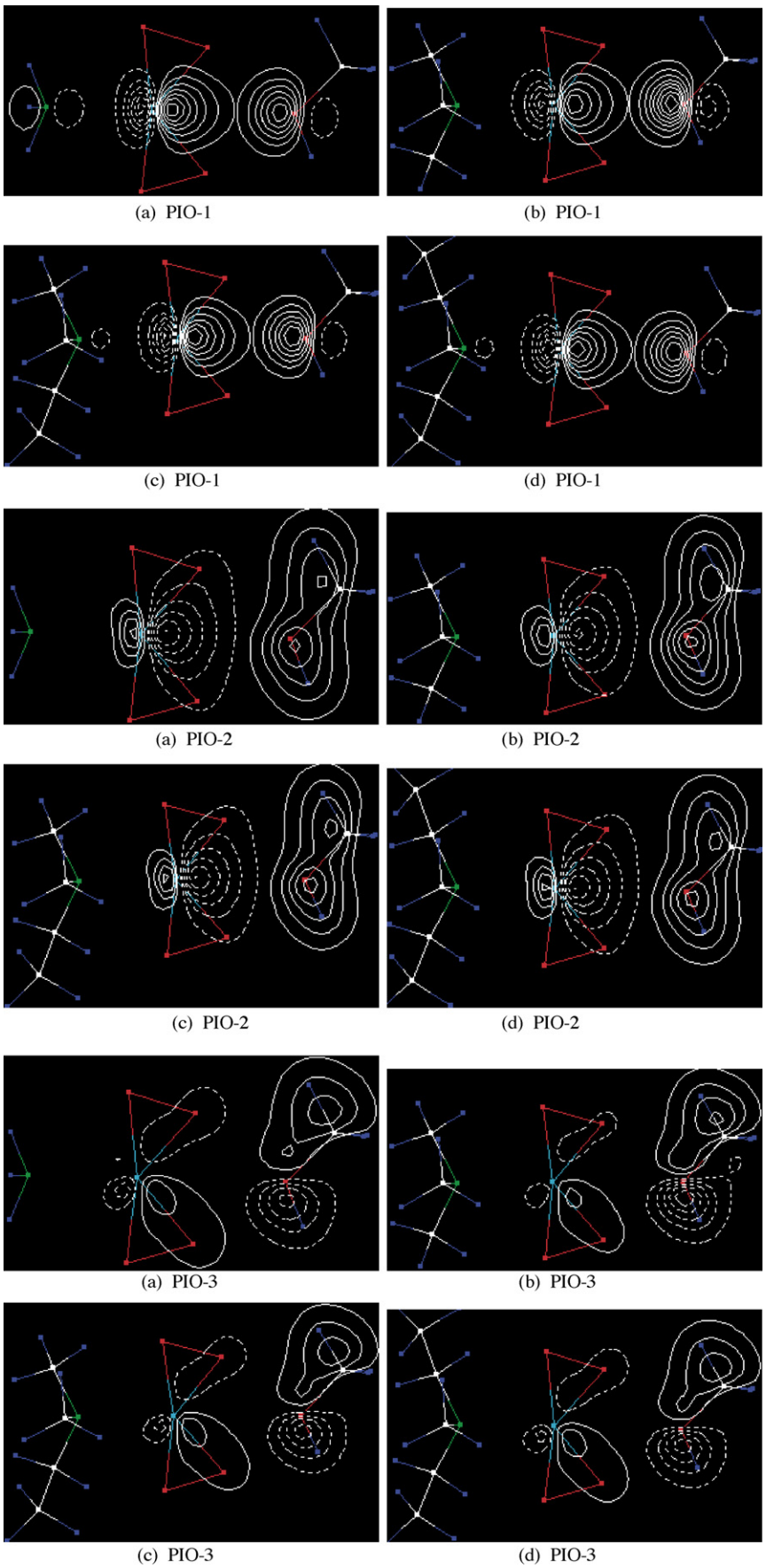

Fig. 4. Contour maps of PIO-1, PIO-2 and PIO-3 of (a) model **(6)**, (b) model **(7)**, (c) model **(8)** and (d) model **(9)**.

Table 6
The overlap populations (OP) of the PIO-1, PIO-2 and PIO-3 of each Mo peroxo methanol complex and each methoxy complex

	PIO-1	PIO-2	PIO-3
(6)	0.0094	−0.0053	−0.0011
(7)	0.0091	−0.0052	−0.0011
(8)	0.0090	−0.0052	−0.0011
(9)	0.0090	−0.0052	−0.0011
(10)	0.2129	0.0021	−0.0080
(11)	0.2119	0.0010	−0.0077
(12)	0.2128	0.0024	−0.0088
(13)	0.2118	0.0009	−0.0077

Contour maps of PIO-1, PIO-2 and PIO-3 of methoxy complexes: models **(10)**, **(11)**, **(12)** and **(13)**, are shown in Fig. 5. They are very similar to each other.

The occupation numbers (ON) of the PIO-1, PIO-2 and PIO-3 of models **(10)**, **(11)**, **(12)** and **(13)** are also summarized in Table 5. They are very close to each other.

The overlap populations of the PIO-1, PIO-2 and PIO-3 of models **(10)**, **(11)**, **(12)** and **(13)** are also summarized in Table 6. They are also very close to each other.

The main components of the linear combination of canonical MO (LCMO) representation of PIO-1(φ'_1, ψ'_1), PIO-2 (φ'_2, ψ'_2), and PIO-3 (φ'_3, ψ'_3) of model **(10)** are shown below. The PIO-1 of model **(10)** indicates that the Mo peroxo parts of the PIO-1 are composed

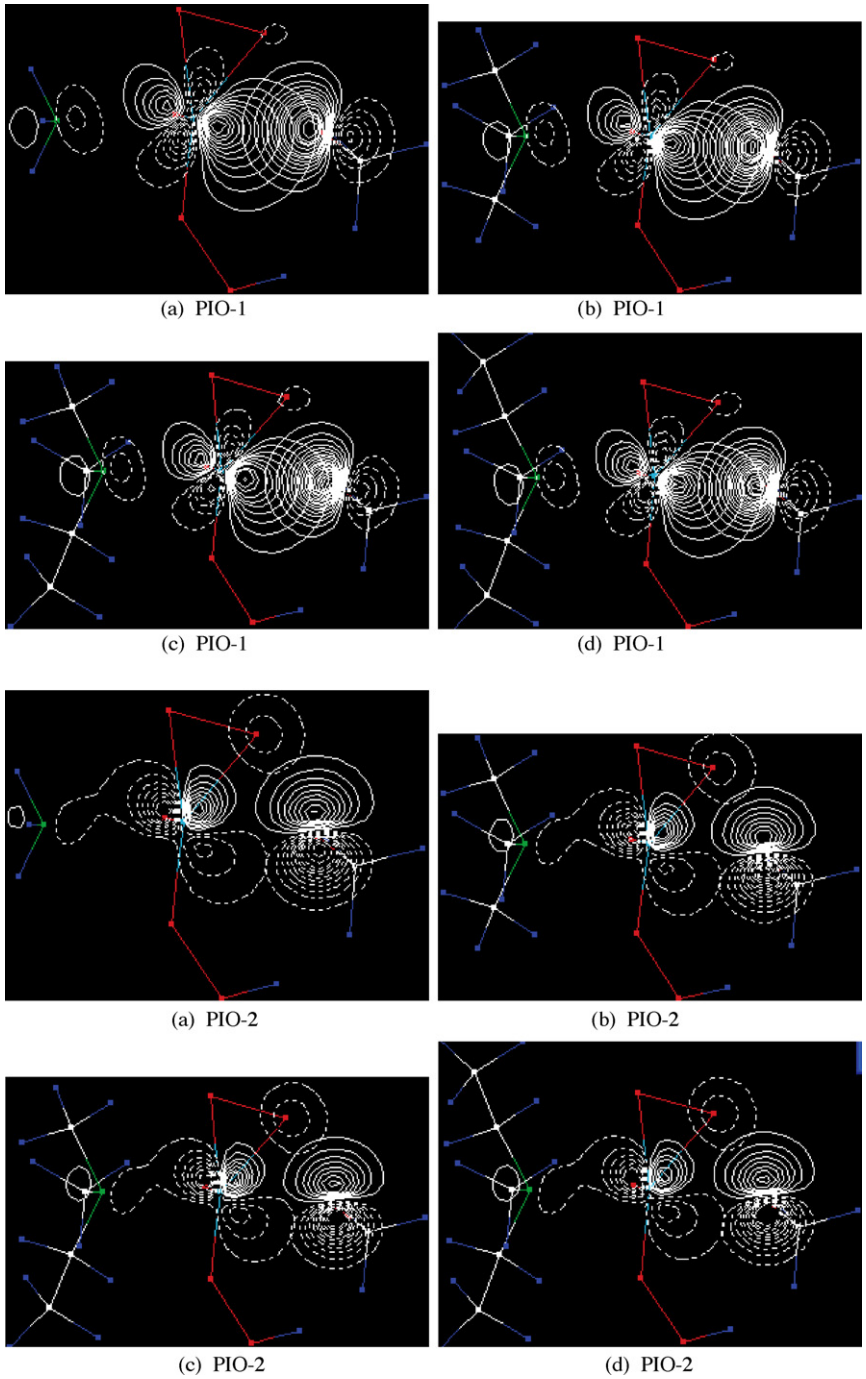

Fig. 5. Contour maps of PIO-1, PIO-2 and PIO-3 of (a) model **(10)**, (b) model **(11)**, (c) model **(12)** and (d) model **(13)**.

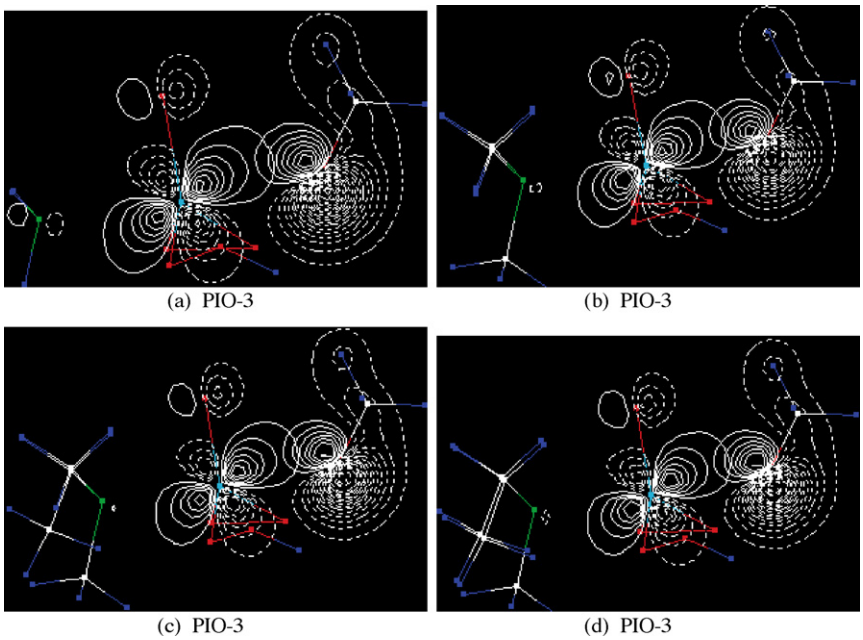

Fig. 5. (*Continued*).

Table 7
The molecular parameters of models **(10)**, **(14)** and **(15)**

	(10)	**(14)**	**(15)**
C–H (Å)	1.107	1.581	1.581
O^5–O^6 (Å)	1.434	1.544	1.544
O^6–H (Å)	3.294	1.581	1.544
<O^5MoO^7 (°)	95.0	95.0	95.0

Table 8
Extended Hückel parameters

Orbital	Hii (eV)	ζ_1	ζ_2
H 1s	−13.60	1.300	
C 2s	−21.40	1.625	
C 2p	−11.40	1.625	
N 2s	−26.00	1.950	
N 2p	−13.40	1.950	
O 2s	−32.30	2.275	
O 2p	−14.80	2.275	
P 3s	−18.60	1.600	
P 3p	−14.00	1.600	
Mo 5s	−8.770	1.960	
Mo 5p	−5.600	1.900	
Mo 4d	−11.06	4.540	0.5899
		1.900	0.5899

of unoccupied orbitals, while the methoxy parts of the PIO-1 are composed of occupied orbitals. The PIO-1 of model **(10)** expresses the electron delocalization from the methoxy group to the Mo peroxo part. On the contrary, the PIO-2 of model **(10)** indicates that the Mo part is composed of many occupied orbitals and several unoccupied orbitals and that the methoxy part is composed of occupied orbitals. The PIO-2 of model **(10)** expresses mixtures of the overlap repulsion between the methoxy part and the Mo peroxo part and electron delocalization from the methoxy part to the Mo peroxo part. The compositions of the PIO-3 of model **(10)** are similar to those of the PIO-2. The characteristics of the PIO-3 and the PIO-2 resemble each other.

Model **(10)** PIO-1: the Mo peroxo part,
$\varphi'_1 = -0.48\varphi_{23}(\mathrm{LUMO}) - 0.44\varphi_{24} - 0.48\varphi_{25} + 0.32\varphi_{26} - 0.37\varphi_{27}$,

Model **(10)** PIO-1: the methoxy part,

$\psi'_1 = -0.22\psi_1 + 0.36\psi_2 + 0.25\psi_3 - 0.70\psi_5 + 0.52\psi_7(\mathrm{HOMO})$.

Model **(10)** PIO-2: the Mo peroxo part,

$\varphi'_2 = 0.24\varphi_5 + 0.22\varphi_{10} - 0.18\varphi_{15} + 0.18\varphi_{19} - 0.15\varphi_{20}(\mathrm{HOMO}-2) - 0.70\varphi_{23}(\mathrm{LUMO}) + 0.29\varphi_{24} - 0.27\varphi_{26}$,

Model **(10)** PIO-2: the methoxy part,

$\psi'_2 = 0.29\psi_1 + 0.47\psi 4 - 0.18\psi_5 + 0.80\psi_6(\mathrm{HOMO\text{-}1})$.

Model **(10)** PIO-3: the Mo peroxo part,

$\varphi'_3 = -0.25\varphi_2 + 0.40\varphi_5 + 0.29\varphi_8 + 0.37\varphi_{10} + 0.32\varphi_{19} + 0.22\varphi_{23}(\mathrm{LUMO}) - 0.48\varphi_{24} + 0.20\varphi_{26} - 0.20\varphi_{27}$,

Model **(10)** PIO-3: the methoxy part,

$\psi'_3 = 0.49\psi_1 + 0.35\psi_3 + 0.40\psi_5 + 0.64\psi_7(\mathrm{HOMO}) + 0.17\psi_8(\mathrm{LUMO}) + 0.18\psi_{10}$.

We compared the LCAO representations of the PIO-1 of model **(10)** with the LCAO representations of the PIO-1 of model **(13)**. They are almost coincident with each other.

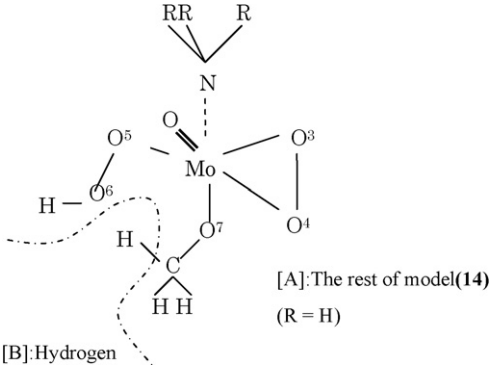

Fig. 6. Schematic illustration of model **(14)**.

Model **(10)** of PIO-1: the Mo peroxo part,
$\varphi'_1 = 0.29\mathrm{Mo5s} + 0.40\mathrm{Mo5p_y} - 0.47\mathrm{Mo4d_{x2-y2}} - 0.29\mathrm{Mo4d_{z2}} + 0.47\mathrm{Mo4d_{xy}} + 0.24\mathrm{Mo4d_{yz}} - 0.24\mathrm{O}^4\mathrm{2s} - 0.27\mathrm{N2p_y}$,
Model **(10)** of PIO-1: the methoxy part,
$\psi'_1 = 0.40\mathrm{O2s} - 0.79\mathrm{O2p_y} - 0.36\mathrm{O2p_z}$,
Model **(13)** of PIO-1: the Mo peroxo part,

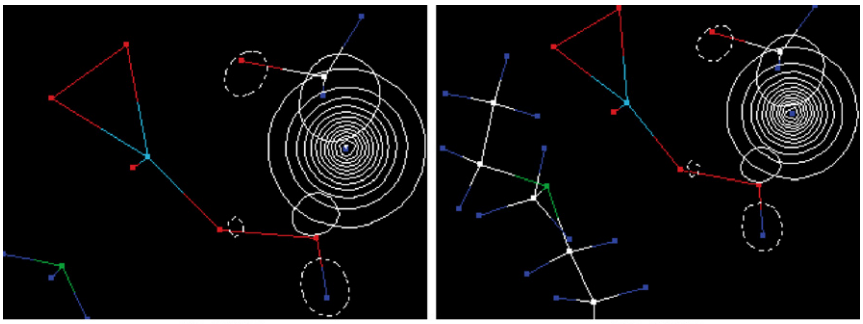

(a) PIO-1 (b) PIO-1

Fig. 7. Contour maps of PIO-1 of (a) model **(14)** and (b) model **(15)**.

$\varphi'_1 = -0.29\mathrm{Mo5s} - 0.41\mathrm{Mo5p}_y + 0.46\mathrm{Mo4d}_{x2-y2} + 0.29\mathrm{Mo4d}_{z2} - 0.47\mathrm{Mo4d}_{xy} - 0.27\mathrm{Mo4d}_{yz} + 0.24\mathrm{O}^4\mathrm{2s} + 0.30\mathrm{N2p}_y$,
Model **(13)** of PIO-1: the methoxy part,
$y'_1 = -0.40\mathrm{O2s} + 0.79\mathrm{O2p}_y + 0.36\mathrm{O2p}_z$,

These results suggest that the influence of amines on the methoxy complex formation is small.

3.2.3. Hydrogen abstraction

We can execute PIO calculations of an assumed intermediate model of methoxy hydrogen abstraction. We start from the Mo peroxo methoxy model **(10)**. We elongate the C–H bond of the methoxy and the O^5–O^6H bond of the hydroperoxo, change the angle of O^5MoO^7, and make the assumed model **(14)**. The bond lengths and the bond angles of the model **(14)** are shown in Table 7. The amine ligand of model **(15)** is NMeEt2.

A schematic illustration of the assumed model **(14)** and the fragmentation of it is shown in Fig. 6. Here, [B] is hydrogen and [A] is the rest of model **(14)**. We have only one PIO, PIO-1, as shown in Fig. 7.

The main components of the LCAO representation of PIO-1 (φ'_1, ψ'_1) of model **(14)** and model **(15)** are as follows:

Model **(14)** of PIO-1: the rest of model **(14)** part,
$\varphi'_1 = 0.10\mathrm{O}^5\mathrm{2p}_x + 0.11\mathrm{O}^5\mathrm{2p}_y + 0.09\mathrm{O}^6\mathrm{2p}_x - 0.08\mathrm{O}^6\mathrm{2p}_y + 0.29\mathrm{O}^7\mathrm{2p}_x - 0.15\mathrm{O}^7\mathrm{2p}_z - 0.29\mathrm{C2s} - 0.58\mathrm{C2p}_x + 0.31\mathrm{C2p}_y + 0.51\mathrm{C2p}_z$,
Model **(14)** of PIO-1: the hydrogen part,
$\psi'_1 = 1.0\mathrm{H1s}$
Model **(15)** of PIO-1: the rest of model **(15)** part,
$\varphi'_1 = 0.09\mathrm{O}^5\mathrm{2p}_x + 0.11\mathrm{O}^5\mathrm{2p}_y + 0.09\mathrm{O}^6\mathrm{2p}_x - 0.08\mathrm{O}^6\mathrm{2p}_y + 0.29\mathrm{O}^7\mathrm{2p}_x - 0.15\mathrm{O}^7\mathrm{2p}_z - 0.29\mathrm{C2s} - 0.58\mathrm{C2p}_x + 0.31\mathrm{C2p}_y + 0.51\mathrm{C2p}_z$,
Model **(15)** of PIO-1: the hydrogen part,
$\psi'_1 = -1.0\mathrm{H1s}$.

PIO-1 (φ'_1, ψ'_1) of model **(14)** coincides with that of model **(15)**. The influence of amines on the hydrogen abstraction is not observed.

4. Discussion

When a reagent and a catalyst approach each other, mutual electron delocalization between the reagent and the catalyst begins to take place and simultaneously overlap repulsion, occupied – occupied orbitals interactions, emerges between the reagent and the catalyst. The electron delocalization should occur to overcome the overlap repulsion in order to proceed a chemical reaction effectively. PIO analysis of an interacting system on the reaction path, for example TS, give us characteristics of several important PIOs which contribute to the interacting system.

We can recognize three important PIOs: PIO-1, PIO-2 and PIO-3, by PIO analysis of model **(2)**, TS of ethylene epoxidation. The characteristic feature of the PIO-1 is the electron delocalization from the π-orbital of the ethylene to the σ*-orbital(O^3–O^4) of the Mo peroxo, that of the PIO-2 is the electron delocalization from the p-orbital of O^4 of the Mo peroxo to the π*-orbital of the ethylene and that of the PIO-3 is the overlap repulsion between the ethylene and occupied (Mo–O^3–O^4) orbitals of the Mo peroxo.

Since the (Mo Mo–O^3–O^4) orbitals are destabilized in the cases of model **(4)** and model **(5)** by the coordination of the higher tertiary alkylamines, the overlap repulsion becomes large and so the contribution of the overlap repulsion on the interacting system markedly increases. As the result, the characteristic feature of the PIO-2 of model **(4)** and that of the PIO-1 of model **(5)** become the overlap repulsion and we suggest that ethylene epoxidation takes place favorably on models **(1)**, **(2)** and **(3)**, while the epoxidation is hindered on models **(4)** and **(5)**.

In the case of methanol oxidation, the main components of the PIO-1 of the methanol coordination and the methoxy complex formation are Mo-4d orbitals of the unoccupied orbitals of the Mo peroxo part, and the main components of the PIO-1 of the hydrogen abstraction are O^5, O^6 and C of 2p orbitals of SOMO of the Mo peroxo part. The energies of MOs, which respectively contain these Mo-4d, O-2p and C-2p orbitals, are not influenced by the coordination of amines on Mo atom. Some researchers suggest that methanol oxidation is not hindered by the coordination of amines on Mo peroxo complexes.

5. Conclusion

Since PIO analysis considers not only frontier orbital interactions but also all other molecular orbital interactions of the system, PIO analysis is a convenient tool for understanding reaction mechanisms and for predicting the reactivity of catalytic systems, especially those large in size. Oxidation mechanisms of ethylene and methanol on $Mo(O)(OO)_2$(amine) are studied. In the case of ethylene oxidation, we executed PIO analyses of the transition states. PIO analysis reveals the electron delocalization from the π-orbital of the ethylene to the σ*-orbital (O^3–O^4) of the Mo peroxo, the so called π-donation of ethylene, the electron delocalization from the p-orbital of O^4 of the Mo peroxo to the π*-orbital of the ethylene, and the overlap repulsion between occupied orbitals of the ethylene and occupied (Mo–O^3–O^4) orbitals of the Mo peroxo. This overlap repulsion is enhanced by the coordination of higher alkyl amines to the Mo peroxo, because of the destabilization of these occupied (Mo–O^3–O^4) orbitals. So, we suggest that ethylene epoxidation is hindered by the coordination of higher alkyl amines. On the contrary, in the case of methanol oxidation, methanol coordination to the Mo peroxo moiety, Mo–methoxy complex formation and hydrogen abstraction, which are elementary reactions of methanol oxidation, are not hindered by the coordination of amines. This is one reason why a selective oxidation of alcohols is attained by addition of higher alkyl amines to the oxidation system.

Acknowledgement

The authors thank Dr. F. S. Howell (Sophia University Professor of Chemistry Department) for his helpful advice.

Appendix A

Coulomb integrals and orbital exponents are listed in Table 8.

References

[1] G. Strukul, Catalytic oxidations with hydrogen peroxide as oxidant, in: Catalysis by Metal Complexes, vol. 9, Kluwer Academic Publishers, Dordrecht/Boston/London, 1992, p. 177.
[2] Y. Kurusu, Y. Masuyama, Polyhedron 5 (2000) 127.
[3] (a) K.A. Jørgensen, R. Hoffman, Acta Chem. Scand. B40 (1986) 411;
(b) K.A. Jørgensen, Chem. Rev. 89 (1989) 431;
(c) C.D. Valentin, P. Gisdakis, I.V. Yudanov, N. Rösch, J. Org. Chem. 65 (2000) 2996;
(d) D.V. Deubel, J. Sundermeyer, G. Frenking, J. Am. Chem. Soc. 122 (2000) 10101;
(e) C.D. Valentin, R. Candolfi, P. Gisdakis, N. Rösch, J. Am. Chem. Soc. 123 (2001) 2365;
(f) P. Gisdakis, I.V. Yudanov, N. Rösch, Inorg. Chem. 40 (2001) 3755;
(g) P. Macchi, A.J. Schultz, F.K. Larsen, B.B. Iversen, J. Phys. Chem. A (2001) 9231;
(h) F.R. Sensato, Q.B. Cass, E. Longo, J. Zukerman-Schpector, R. Custodio, J. Andres, M.Z. Hernandes, R.L. Longo, Inorg. Chem. 40 (2001) 6022;
(i) D.V. Deubel, G. Frenking, P. Gisdakis, W. Herrmann, N. Rosch, J. Sundermeyer, Acc. Chem. Res. 37 (2004) 645;
(j) F.R. Sensato, R. Custodio, E. Longo, V.S. Safont, J. Andres, Eur. J. Org. Chem. 2005 (2005) 2406.
[4] (a) L. Deng, T. Ziegler, Organometallics 15 (1996) 3011;
(b) L. Deng, T. Ziegler, Organometallics 16 (1997) 716.
[5] http://classic.chem.msu.su/gran/gamess/index.old.html.
[6] (a) H. Fujimoto, T. Yamasaki, H. Mizutani, N. Koga, J. Am. Chem. Soc. 107 (1985) 6157;
(b) H. Fujimoto, Acc. Chem. Res. 20 (1987) 448.
[7] T. Motoki, A. Shiga, J. Computational Chem., 25 (2004) 106 LUMMOX™, sold by Ryouka System Inc. (Tokyo), correspondent K. Chiba e-mail: chibao@rsi.co.jp http://www.rsi.co.jp/kagaku/cs/pio/index.html.
[8] (a) A. Shiga, Y. Kurusu, J. Mol. Catal. A 241 (2005) 199;
(b) T. Motoki, A. Shiga, J. Comput. Chem. 25 (2004) 106.
[9] (a) A. Shiga, J. Kojima, T. Sasaki, Y. Kikuzono, J. Organometal. Chem. 345 (1988) 275;
(b) A. Shiga, H. Kawamura, T. Ebara, T. Sasaki, Y. Kikuzono, J. Organometal. Chem. 366 (1989) 95;
(c) A. Shiga, J. Macromol. Sci. A34 (1997) 1867;
(d) A. Shiga, J. Mol. Catal. A 146 (1999) 325;
(e) J. Handzlik, A. Shiga, J. Kondziolka, J. Mol. Catal. A 284 (2008) 8.